Journal of Sound and Vibration (2000) **233**(3), 407–422
doi:10.1006/jsvi.1999.2816, available online at http://www.idealibrary.com on IDEAL®

A SYMMETRIC FORMULATION OF COUPLED BEM/FEM IN SOLVING RESPONSES OF SUBMERGED ELASTIC STRUCTURES FOR LARGE DEGREES OF FREEDOM

P.-T. CHEN

Department of Naval Architecture, National Taiwan Ocean University, Keelung, Taiwan, Republic of China

S.-H. JU

National Cheng-kung University, Tainan, Taiwan, Republic of China

AND

K.-C. CHA

Chung-Shan Institute of Science and Technology, Tauyuan, Taiwan, Republic of China

(*Received* 3 *February* 1999, *and in final form* 11 *October* 1999)

This work presents a symmetric formulation for the coupling of boundary element method (BEM) with finite element method (FEM) to compute responses of submerged elastic structures in a heavy acoustic medium. The acoustic loading derived from BEM is formulated in a symmetric complex matrix. The symmetry of the acoustic loading matrix is proven by an acoustic reciprocal principle, which relate two sets of arbitrary surface normal velocities and surface pressures in terms of surface integrals. The structural equation is represented by FEM. The fact that the acoustic loading and the structural equation are symmetric allows us to take the storage and computational advantages of the banded matrix which has been widely used in conventional finite element methods. Consequently, the computational efficiency of the proposed coupled FEM/BEM is significantly increased. The proposed method involving 20 000 degrees of freedom can be implemented on a personal computer. Numerical results are verified by analytical solutions of a constant thickness spherical shell subject to a point alternating force as well as the previously published variational solution of a constant thickness spheroidal shell excited by a concentrated force.

1. INTRODUCTION

The coupled finite element method/boundary element method (FEM/BEM) is a conventional means of computing responses for an arbitrarily elastic structure submerged in a fluid subjected to alternating external forces. The FEM is used to describe the dynamic behavior of the structure, while the BEM is used to represent the surface acoustic loading on the structure. The coupling boundary conditions between the fluid and structure are the continuity of wetted surface normal velocity and the surface pressure acting as a loading on the structure. The standard approach to handling the structural equation in coupling with the acoustic equation is to eliminate the structural displacement variables from the two equations. By doing so, one obtains an equation which only contains the surface pressure as the unknown variable to describe the coupled structural/acoustic system [1, 2]. Jeans and Mathews [3] used a variational formulation to the normal derivative of a surface boundary integral equation to deal with thin shells submerged in a fluid. The equation governing the

0022-460X/00/230407 + 16 $35.00/0

response is a symmetrically complex matrix using the pressure as a variable. Everstine and Henderson [4] coupled the surface pressure loading, represented by a Helmholtz integral equation, with a NASTRAN program which modelled elastic structures. That investigation also implemented an out-of-core solver to resolve large-scale problems. Everstine [5] also applied coupled FEM/BEM to deal with low-frequency resonances by treating added mass derived from the boundary integral equation at low-frequency limits. The matrix associated with the added mass, although lacking a formal derivation, is identified as symmetric.

Despite their merits, the above investigations are severely limited by the large number of degrees of freedom in large-scale problems because the derivations of the coupled equations involve matrix inversions of structural displacement variables for which the displacement variables are eliminated. Also, the matrices associated with BEM are not symmetric in some formulations. The degrees of freedom of the matrix inversions are of the order of structural degrees of freedom, which are generally six times the number of structural nodal points, and the inverted matrices are fully populated. Such inversions require massive memory storage and computational capacity, leading to the limitation for large-scale problems. In reference [5], the execution of a problem having 16 000 degrees of freedom requires many hours of supercomputer time. For conventional finite element methods used to form the matrix equations, the banded nature of the matrix storage leads to tremendous savings in memory allocation and computational capacity, thereby providing efficient numerical implementations. Nevertheless, the banded nature of matrix storage could not be directly employed by the conventional FEM/BEM schemes as discussed above.

Chen and Ginsberg [6] demonstrated that the acoustic loading on the wetted surface is a complex symmetric matrix by a surface acoustic reciprocal principle. The symmetry of the acoustic loading serves as the basis for this work to formulate an efficient coupled BEM/FEM. The paper presents a numerical method capable of taking advantage of the banded nature of the finite element method and the symmetry of the acoustic loading, thus leading to savings in memory storage and efficient numerical execution dramatically. The computation is implemented on a PC with Pentium II CPU.

2. COUPLED EQUATION FOR BEM/FEM

The coupling boundary condition for the coupled structural equation and acoustic equation is the continuity of the normal velocities on the wetted surface of these two equations. Therefore, the degrees of freedom for the structural equation are established in such a manner that the three linear displacement components of the nodal points on the wetted surface are oriented in normal and tangential directions to the surface. Rotational displacements and nodal points other than on the wetted surface could be arbitrarily oriented, such as the global co-ordinate directions for convenience. If $[\hat{k}_e]$ denotes an elementary stiffness matrix defined in a global co-ordinate system, then the stiffness matrix $[k_e]$ oriented to the normal surface direction is

$$[k_e] = T^{\mathrm{T}}[\hat{k}_e]\,T, \tag{1}$$

where the superscript "T" represents matrix transpose. The element transformation T can be expressed as

$$T = \begin{bmatrix} \phi_i & & & & 0 \\ & I & & & \\ & & \phi_j & & \\ & & & \ddots & \\ 0 & & & & I \end{bmatrix}, \tag{2}$$

where ϕ_i and ϕ_j are proper 3×3 directional cosine matrices for linear displacements on the wetted surface between the global co-ordinate system and normal surface directions, respectively, I is a unit 3×3 identity matrix corresponding to those nodal points not on the surface or to the rotational displacements. The total stiffness matrix $[k]$ is formed by summing up the elementary matrices:

$$[k] = \sum_e [k_e]. \tag{3}$$

The total stiffness matrix can then be partitioned into the surface normal degree of freedom as denoted by a subscript symbol "n" and the remaining degrees of freedom by "i", which include the surface tangent displacements, the interior nodal points not in contact with the fluid, and all the rotational displacements:

$$[k] = \begin{bmatrix} k_{nn} & k_{ni} \\ k_{in} & k_{ii} \end{bmatrix}. \tag{4}$$

Correspondingly, the submerged structural equation subject to the acoustic loading and external forces oscillating at a frequency ω is

$$\left(\begin{bmatrix} k_{nn} & k_{ni} \\ k_{in} & k_{ii} \end{bmatrix} - \omega^2 \begin{bmatrix} M_{nn} & M_{ni} \\ M_{in} & M_{ii} \end{bmatrix} \right) \begin{Bmatrix} x_n \\ x_i \end{Bmatrix} = \begin{Bmatrix} f_n \\ f_i \end{Bmatrix} + \begin{Bmatrix} -[N]^{\mathrm{T}} P \\ 0 \end{Bmatrix}, \tag{5}$$

where M_{pq} $(p, q = n, i)$ are global mass matrices corresponding to the n and i degrees of freedom, x_n and x_i are the corresponding displacement variables, f_n and f_i are the associated external alternating forces, P is the discretized surface pressure, and N is a shape factor matrix arising from shape functions in discretizing the normal displacement and surface pressure. The shape factor matrix can be identified by considering the virtual work δW done by the surface pressure against the structure's virtual normal displacement δw:

$$\begin{aligned} \delta W = \int_S P \delta w \, \mathrm{d}s &= \int_S \left[\sum_e \left(\sum_i P_i \psi_{i,e} \right) \right] \left[\sum_e \left(\sum_j \delta X_{n,j} \phi_{j,e} \right) \right] \mathrm{d}s \\ &= \sum_i \sum_j P_i \delta X_{n,j} \int_S \left(\sum_e \psi_{i,e} \right) \left(\sum_e \phi_{j,e} \right) \mathrm{d}s \\ &= \sum_i \sum_j P_i \delta X_{n,j} N_{ij}, \end{aligned} \tag{6}$$

where $\psi_{i,e}$ and $\phi_{j,e}$ are the shape functions for pressure and normal displacement, and the expression $\sum_e (\sum_i P_i \psi_{i,e})$ is the interpolated pressure on the surface in terms of the nodal pressure P_i. The inner summation denotes a contribution of the interpolated pressure form an individual element, while the outer summation represents the contribution from all the elements on the surface. A similar expression can be used for the displacement. The coefficients N_{ij} are the coefficients of the shape factor matrix N.

The surface acoustics relating the surface pressure and normal derivative of the surface pressure is described by a boundary Helmholtz integral equation:

$$(1 - \Omega(x)) P(x) = \int (P(y) \frac{\partial G(x, y)}{\partial n(y)} - \frac{\partial P(y)}{\partial n(y)} G(x, y)) \, \mathrm{d}S_y, \tag{7}$$

where x is a field point, y is a source point, dS_y is the differential area integrating with respect to source point y, $\partial P/\partial n$ is the pressure normal derivative, and $G(x, y)$ is the free-space Green's function

$$G(x, y) = \frac{e^{-ik|x-y|}}{4\pi|x-y|} \tag{8}$$

in which k is a wave number defined as $k = \omega/c$, and c is the sound velocity. The $\Omega(x)$ is defined by

$$\Omega(x) = -\frac{1}{4\pi}\int \frac{\partial(1/|x-y|)}{\partial n(y)}\, dSy \tag{9}$$

which is the solid angle at point x subtended over the wetted surface of the interior domain. Note that the oscillation time factor is $e^{i\omega t}$. The pressure normal derivative relates to the normal displacement as

$$\frac{\partial P}{\partial n} = \rho_0 \omega^2 x_n, \tag{10}$$

where ρ_0 is the fluid density. Discretizing P and $\partial P/\partial n$ in equation (7) leads to the matrix equation,

$$[H]\{P\} = [G]\left\{\frac{\partial P}{\partial n}\right\}, \tag{11}$$

where $\{P\}$ and $\{\partial P/\partial n\}$ are discretized nodal values, and $[H]$ and $[G]$ are complex matrices. By combining equations (10) and (11), the surface pressure $\{P\}$ relates to the normal displacement $\{X_n\}$ as

$$\{P\} = [H]^{-1}[G](\rho_0\omega^2)\{x_n\}. \tag{12}$$

Substituting the above equation into equation (5) leads to the equation for forced vibration of the submerged structure:

$$\begin{bmatrix} D_{nn} & D_{ni} \\ D_{in} & D_{ii} \end{bmatrix}\begin{Bmatrix} x_n \\ x_i \end{Bmatrix} + \begin{bmatrix} \rho_0\omega^2[N]^{\mathrm{T}}[H]^{-1}[G] & 0 \\ 0 & 0 \end{bmatrix}\begin{Bmatrix} x_n \\ x_i \end{Bmatrix} = \begin{Bmatrix} f_n \\ f_i \end{Bmatrix}$$

or in short symbol

$$[K_G]\{X\} = \{F\}, \tag{13}$$

where K_G is the sum of the above two matrices, and D_{pq} $(p, q = i, n)$ are identified as

$$D_{pq} = K_{pq} - \omega^2 M_{pq}. \tag{14}$$

The second term of the first equation in equation (13) is the acoustic loading which only applies to the normal displacement x_n. The effects of the acoustic loading on x_i is through the matrices D_{ni} and D_{in}. Equation (13) reveals that the acoustic loading is equivalent to an additional complex stiffness matrix on the normal degree of freedom.

It is worthwhile to review conventional ways to handle the coupling of the structural equation, equation (5), with the acoustic equation, equation (11). Let the above two

equations be written as

$$\begin{bmatrix} D_{nn} & D_{ni} \\ D_{in} & D_{ii} \end{bmatrix} \begin{Bmatrix} x_n \\ x_i \end{Bmatrix} + \begin{bmatrix} N^{\mathrm{T}}\{P\} \\ 0 \end{bmatrix} = \begin{bmatrix} f_n \\ f_i \end{bmatrix}, \qquad HP = \rho_0 \omega^2 G[I \;\; 0] \begin{bmatrix} x_n \\ x_i \end{bmatrix}, \tag{15}$$

where I is an identity matrix having the dimension consistent with the variable x_n, and the unknown variables are $\{x_n\}$, $\{x_i\}$ and $\{P\}$. The variables can be obtained by solving the above two equations simultaneously, but the associated matrix of the equation has a large dimension, requiring huge memory storage for large-scale problems. One way to deal with such a situation is to express the displacement $\{x_n\}$ and $\{x_i\}$ in terms of pressure variable $\{P\}$ from the first matrix equation, and then to substitute into the second equation, leading to a matrix equation containing only pressure $\{P\}$ as the unknown variable. This displacement variables elimination process involves structural matrix inversion, and matrix multiplications, requiring massive memory allocation and computation capacity. Instead of using the conventional ways, the present method treats the acoustic loading in equation (13) as an acoustic element. The element is examined in the following section.

3. ACOUSTIC LOADING MATRIX

The surface complex power $\boldsymbol{P}$, which is defined as one half of the surface integral of the surface pressure P, multiplying the complex conjugate of the normal velocity v_n^*, is computed as

$$\begin{aligned} \boldsymbol{P} &= \frac{1}{2} \int P v_n^* \, \mathrm{d}S = \frac{1}{2} \int \left[\sum_e \left(\sum_i P_i \psi_{i,e} \right) \right] \left[\sum_e \left(\sum_j v_j^* \phi_{j,e} \right) \right] \mathrm{d}S \\ &= \frac{1}{2} \sum_i \sum_j P_i v_j^* \int \left(\sum_e \psi_{i,e} \right) \left(\sum_e \phi_{j,e} \right) \mathrm{d}S = \frac{1}{2} \sum_i \sum_j P_i v_j^* N_{ij}, \end{aligned} \tag{16}$$

where the surface pressure and normal velocity are discretized by the shape functions used in equation (6). Substituting equation (11) into the pressure variable P_i of the above equation and relating $\partial P/\partial n$ to the normal displacement x_n in equation (10), we have the surface complex acoustic power expressed in terms of x_n:

$$\boldsymbol{P} = \tfrac{1}{2}(-\mathrm{i}\omega)\rho_0 \omega^2 \{x_n^*\}^{\mathrm{T}} [N]^{\mathrm{T}} [H]^{-1} [G] \{x_n\} \tag{17}$$

which is a quadratic form of the matrix $\rho_0 \omega^2 [N]^{\mathrm{T}} [H]^{-1} [G]$. This matrix is identical to the acoustic loading matrix in equation (13). In a previous study [6], the surface complex power obtained by an assumed modes expansion for the surface normal velocity is a quadratic form of the velocity expansion coefficients whose corresponding matrix is symmetric. The present matrix $\rho_0 \omega^2 [N]^{\mathrm{T}} [H]^{-1} [G]$ arising from the shape function discretization can also be proved to be symmetric.

The foundation of the matrix symmetry is based on an acoustic reciprocal principle [6] for a body immersed in an infinite extent acoustic medium and that for two arbitrary sets of surface velocities and pressure distributions P_1, V_1, and P_2, V_2, the following relation holds:

$$\int P_1 V_2 \, \mathrm{d}S = \int P_2 V_1 \, \mathrm{d}S. \tag{18}$$

The approximated pressures $\bar{P}_1$ and $\bar{P}_2$ can be interpolated by nodal values $P_{1,i}$ and $P_{2,i}$:

$$\bar{P}_1 = \sum_e \left(\sum_i P_{1,i} \psi_{i,e} \right), \qquad \bar{P}_2 = \sum_e \left(\sum_i P_{2,i} \psi_{i,e} \right) \tag{19}$$

and the approximated velocities $\bar{v}_1$ and $\bar{v}_2$, by the nodal velocities $v_{1,i}$ and $v_{2,i}$:

$$\bar{v}_1 = \sum_e \left(\sum_i v_{1,i} \phi_{i,e} \right), \qquad \bar{v}_2 = \sum_e \left(\sum_i v_{2,i} \phi_{i,e} \right). \tag{20}$$

The discretized variables $P_{1,i}$, $v_{1,i}$, and $P_{2,i}$, $v_{2,i}$ are related by the matrix equation in equation (11). The approximated quantities $\bar{P}_1$, $\bar{v}_1$ and $\bar{P}_2$, $\bar{v}_2$ approach the exact values P_1, v_1 and P_2, v_2 when the meshes become close to each other. Implement equation (18) numerically using the approximated quantities in equations (19) and (20), leading to

$$\sum_i \sum_j P_{1,i} v_{2,j} \int \left(\sum_e \psi_{i,e} \right) \left(\sum_e \phi_{j,e} \right) \mathrm{d}S = \sum_i \sum_j P_{2,i} v_{1,j} \int \left(\sum_e \psi_{i,e} \right) \left(\sum_e \phi_{j,e} \right) \mathrm{d}S, \tag{21}$$

where the quantities of the integrals are identified as N_{ij}. Consequently, we have the discretized expression for the reciprocal principle of equation (18) as

$$\sum_i \sum_j P_{1,i} v_{2,j} N_{ij} = \sum_i \sum_j P_{2,i} v_{1,j} N_{ij} \tag{22}$$

which can be further expressed containing only nodal velocity variables by using equation (11) to eliminate the pressure variables. Thus, combining equations (22) and (11) leads to

$$\{v_1\}^{\mathrm{T}} ([H]^{-1}[G])^{\mathrm{T}} N \{v_2\} = \{v_2\}^{\mathrm{T}} ([H]^{-1}[G])^{\mathrm{T}} N \{v_1\}, \tag{23}$$

where $\{v_1\}$ and $\{v_2\}$ are the nodal velocities. Because the velocities $\{v_1\}$ and $\{v_2\}$ are arbitrary, equation (23) leads to

$$N^{\mathrm{T}} [H]^{-1} [G] = (N^{\mathrm{T}} [H]^{-1} [G])^{\mathrm{T}} \tag{24}$$

which proves that the acoustic loading matrix in equation (13) is symmetric. For monofrequency oscillations, the phase of surface pressure leads the phase of surface normal velocity, implying that the imaginary part of the product pv_n^* is positive (the oscillating time factor is $\mathrm{e}^{\mathrm{i}\omega t}$). The real part of pv_n^* is also positive owing to the positive power emitting from the surface. Hence, the real and imaginary parts of $\boldsymbol{P}$ in equation (15) are positive. Also, because the symmetry shown in equation (24), denotes

$$N^{\mathrm{T}} [H]^{-1} [G] = \Gamma_R + \mathrm{i}\Gamma_I, \tag{25}$$

where Γ_R and Γ_I are symmetric real matrices, the complex surface power in equation (17) can be written as

$$\boldsymbol{P} = \tfrac{1}{2}(-\mathrm{i}\omega)\rho_0 \omega^2 \{x_n\}^{*\mathrm{T}} \Gamma_R \{x_n\} + \tfrac{1}{2}(-\mathrm{i}\omega)\rho_0 \omega^2 (i) \{x_n\}^{*\mathrm{T}} \Gamma_I \{x_n\}. \tag{26}$$

The real part of $\boldsymbol{P}$ is associated with the second term, while the first term corresponds to the imaginary part of the power. Owing to the positiveness of both the real and the imaginary parts of P, equation (26) indicates that Γ_R is negative definite and Γ_I is positive definite. This observation obviously reveals that the acoustic loading matrix in equation (13) presents inertia effects due to Γ_R and damping effects due to Γ_I. The damping effects are responsible

for radiating power into far fields. This acoustic loading matrix can be viewed as a complex acoustic finite element attached to the structural equation with the continuity of the wetted surface normal displacement. The acoustic finite element, derived from the boundary Helmholtz integral equation of equation (7), fully characterizes the acoustic loading effects on the structure. In the following, the above observation of the symmetry complex acoustic loading finite element is used to implement numerical computations.

The above formulation for the acoustic loading element stems from boundary integral equations. The boundary integral equation of equation (7) fails at frequencies coincident with the interior cavity frequencies of homogeneous Dirichlet boundary conditions. The discretized equation of the $[H]$ matrix in equation (11) becomes ill-conditioned when the exciting frequency is close to the interior frequencies, thus providing an erroneous acoustic loading matrix. This problem could be overcome by using the CHIEF [7] or Burton–Miller method [8] which makes the matrix $[H]$ invertible.

4. COMPUTATIONAL ASPECTS OF THE SUBMERGED STRUCTURAL EQUATION

This study implements numerical computations by applying the sky-line method (variable-bands storage method) and using the Cuthill–Mckee algorithm [9] to reduce the storage bandwidth. The sky-line algorithm is a conventional means of solving real or complex matrix equations. The underlying concept of this method is that only the components below the first non-zero component in each column change after the Cholesky decomposition; thus, only these components should be stored and calculated. The efficiency of this method is highly dependent on the bandwidths of the matrix. A renumbering procedure [9] is normally used to minimize bandwidths before solving the equations. Steps of sky-line method are described as follows.

(1) *Identify the sky-line shape*: For this method, only the components below the first non-zero component in each column are stored into a one-dimensional array S. An index array, LL, is used to indicate the position numbers in the array that correspond to the diagonal elements of the two-dimensional matrix. The last LL represents the total number of complex values required for the global stiffness matrix. Figure 1 presents an illustrative example.

j	1	2	3	4	5	6	7	8	9	10	
$LL(j)$	1	3	5	9	12	15	21	23	29	32	i

$$\begin{bmatrix}
S1 & & & & & & & & & & 1\\
S2 & S3 & & & & & & & & & 2\\
0 & S4 & S5 & & & & & & & & 3\\
S6 & S7 & S8 & S9 & & & \text{Symmetric} & & & & 4\\
0 & 0 & S10 & S11 & S12 & & & & & & 5\\
0 & 0 & 0 & S13 & S14 & S15 & & & & & 6\\
0 & S16 & S17 & S18 & S19 & S20 & S21 & & & & 7\\
0 & 0 & 0 & 0 & 0 & 0 & S22 & S23 & & & 8\\
0 & 0 & 0 & S24 & S25 & S26 & S27 & S28 & S29 & & 9\\
0 & 0 & 0 & 0 & 0 & 0 & 0 & S30 & S31 & S32 & 10
\end{bmatrix}$$

Figure 1. Array structure of sky-line method.

(2) *Form the global stiffness matrix* $[K_G]$: Since the global stiffness matrix is symmetric, only the lower matrix (Figure 1) requires to be stored in the one-dimensional array S. The relationship between the full two-dimensional array $[K_G]$ and the sky-line one-dimensional array, S, is

$$[K_G](i, j) = S(LL(i) + j - i), \quad \text{for } i \geqslant j.$$

(3) *Decompose the matrix* $[K_G]$ *by the Cholesky method*: The decomposition is

$$[K_G] = LDL^{\mathrm{T}},$$

where L is the lower triangular matrix and D is the diagonal matrix.

(4) *Perform forward and backward substitutions to obtain the solution.*

5. NUMERICAL EXAMPLES

Numerical examples are presented by selecting constant thickness spherical and spheroidal shells under concentrated external forces. The point-concentrated forces are more severe computational circumstances than surface loadings. Previous literature provides the analytical solution for the spherical shell [10]. Numerical data for the spheroidal shells were computed by variational formulations published elsewhere [11] in which the acoustic loading was formulated by a surface variational principle and the structural equation was derived by Hamilton's principles. In that formulation, the displacements of the structure and the surface pressure were expanded by a set of assumed expansion functions. Thus, the variational expression of the formulation becomes a function of the expansion coefficients. The equation of the expansion coefficients can be obtained when virtual increments were applied to the displacements and surface pressure for the variational expression. The convergence of the computed results is ensured by the assumed basis amplitude coefficients approaching zero when using a sufficient number of expansion terms. Thus, the variational formulations can be regarded as a numerical/analytical method whose results are satisfactory for numerical comparisons. The material data for the spherical shell are listed as follows: the radius of the shell is 1 m, the thickness of the shell is 0·03 m, Young's modulus is $2{\cdot}07 \times 10^{11}$ Pa (N/m^2), the Poisson ratio is 0·3, the density of the shell and water are 7669 and 1000 kg/m^3, respectively, and the sound speed of the water is 1524 m/s. An external concentrated alternating force is exerted at one apex. To demonstrate the efficiency of using the sky-line memory storage in forming equation (13), we use a full model of mesh generation for the spherical shell. Figure 2 depicts the element meshes. There are 3235 nodal points and 19410 degrees of freedom. The shell elements are based on classical bending plus membrane theories. Initially, we compute the acoustic loading element $\rho_0\omega^2 N^{\mathrm{T}}[H]^{-1}[G]$ and then solve the displacement variables x_n and x_i from equation (13). Because the response is axisymmetric, we plot the normal displacement along the arclength of a generator which generates the surface of the sphere by revolving around a symmetric axis. Figure 3 compares the present method with the analytical solutions [10] where the apex corresponds to zero arclength. The non-dimensionalized frequencies ka are 1·6 and 2·4. Once the x_n is known, the surface pressure is computed accordingly by equation (12) which is persented in Figure 4. Figure 5 illustrates the radiation patterns on the plane cutting through the arclength, where the radiation pattern is computed by an integral formula

$$P(x) = \int \left(P(y) \frac{\partial G(x, y)}{\partial n(y)} - \frac{\partial P(y)}{\partial n(y)} G(x, y) \right) \mathrm{d}Sy, \tag{27}$$

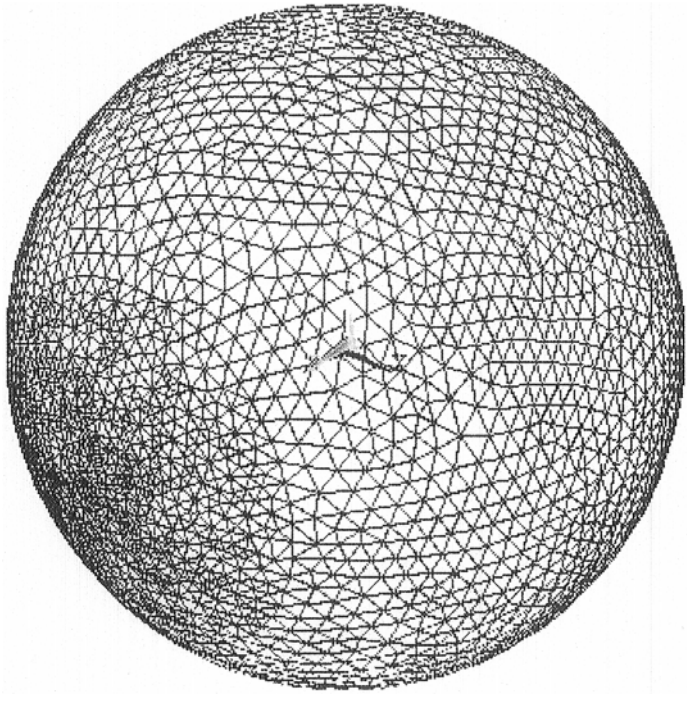

Figure 2. Finite element meshes for a spherical shell.

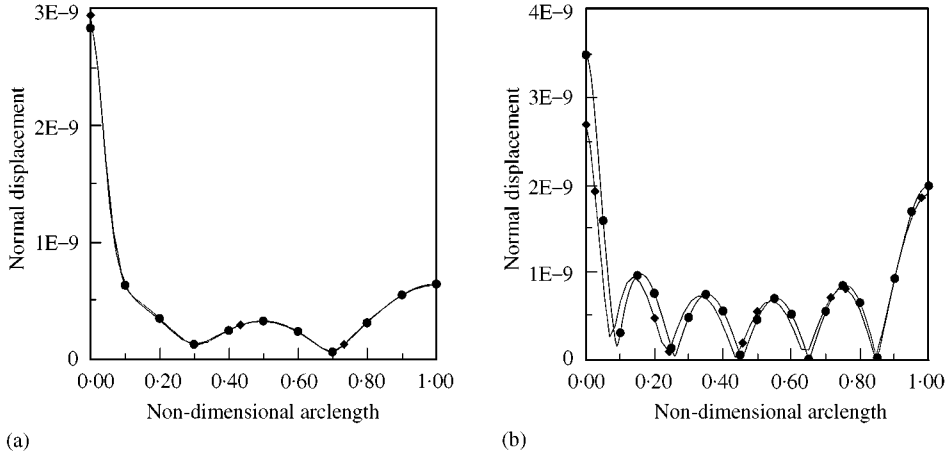

Figure 3. Normal displacement along the arclength of a generator of the spherical shell: (a) $ka = 1{\cdot}6$, (b) $ka = 2{\cdot}4$. –●– Analytical solution; –◆– present analysis.

where the field point x is assigned to a large distance value, factoring out the simple source term $e^{-ik|x|}/|x|$. The symbol "| |" denotes the distance of the field point from the origin. According to Figures (3)–(5), the numerical results for ka being 1·6 closely correspond to the analytical solutions, while some discrepancies are displayed when ka equals 2·4. The errors could be reduced by further refining the meshes. Figures 6 and 7 show the normal displacement and surface pressure at a position of the apex of the applied force versus

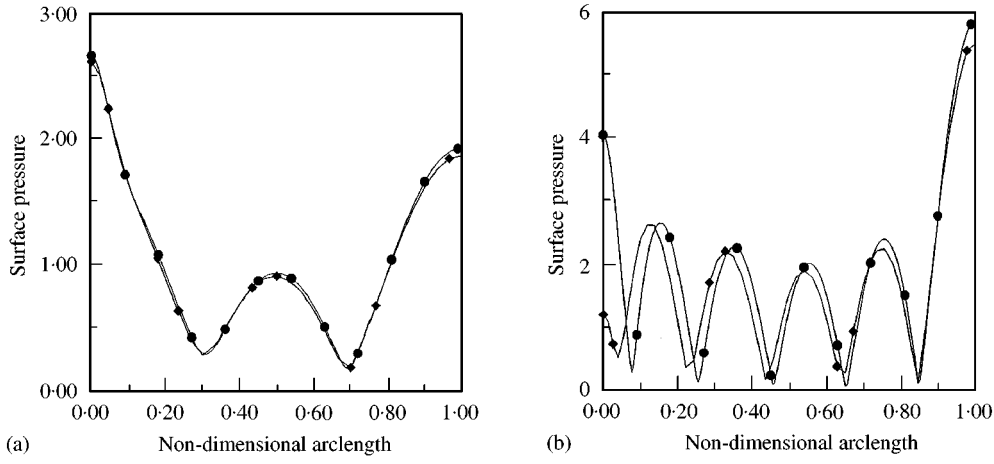

Figure 4. Surface pressure along the arclength of a generator of the spherical shell: (a) $ka = 1{\cdot}6$, (b) $ka = 2{\cdot}4$. –●– Analytical solution; –◆– pressure method.

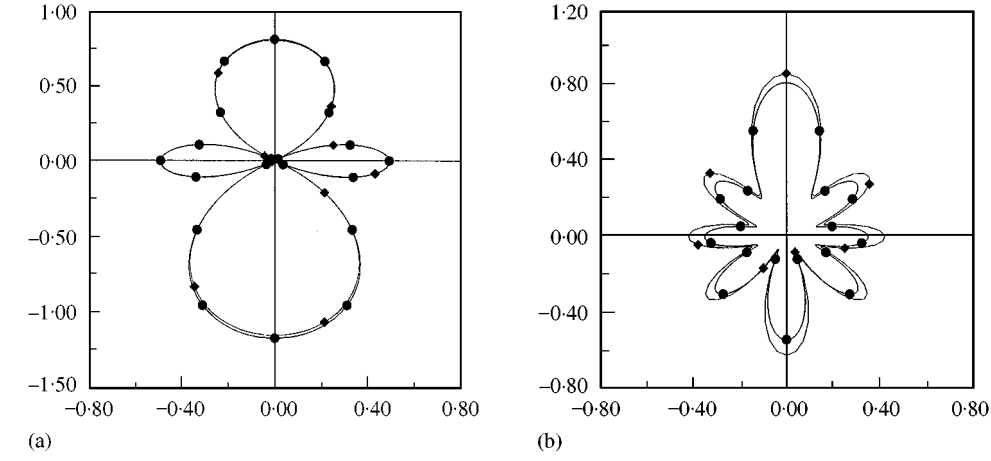

Figure 5. Radiation patterns of the spherical shell: (a) $ka = 1{\cdot}6$, (b) $ka = 2{\cdot}4$. –●– Analytical solution; –◆– present analysis.

scanning exciting frequencies. Also computed herein is the radiated power shown in Figure 8 by taking the real part of the complex surface power in equation (17) or (26).

Next, we present a slender spheroidal shell whose aspect ratio of major radius to minor radius is four. The material data and the ratio of shell thickness to the minor radius are identical to those of the spherical shell studied in the last example. The numerical data used for comparison are computed by using variational formulations to the surface loading and structure vibrations [11]. The external exciting source is a point force applied at one of the two apexes of the shell. Figure 9 depicts the discretized meshes which have 2634 nodal points and 15 804 degrees of freedom. Figure 10 compares the surface normal displacements along the arclength of a generator. Figure 11 displays the corresponding surface pressures. Figure 12 shows the radiation patterns which are laid on the plane containing the arclength. Some discrepancies are observed for ka equal to 2·4. The exciting frequencies were also

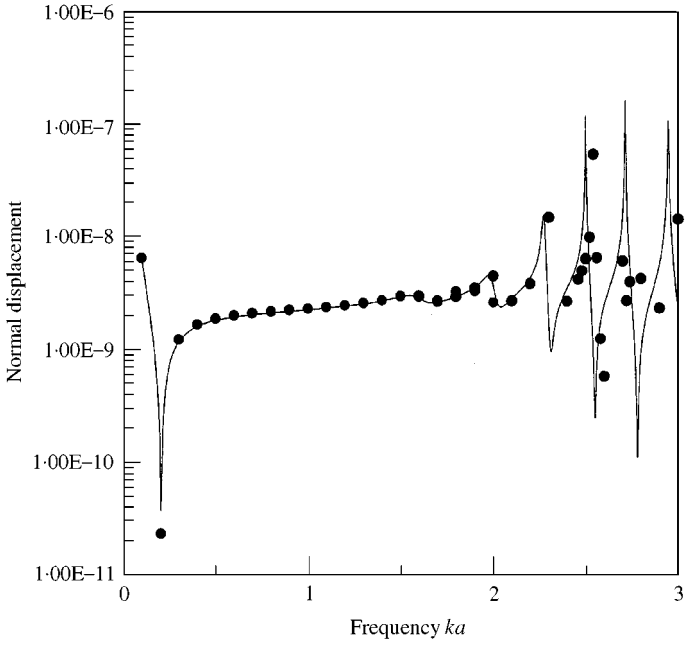

Figure 6. Normal displacement at the apex of the applied point force for the spherical shell versus scanning frequency *ka*. The dotted points are the sampled *ka* values. —— Analytical solution; ● present method.

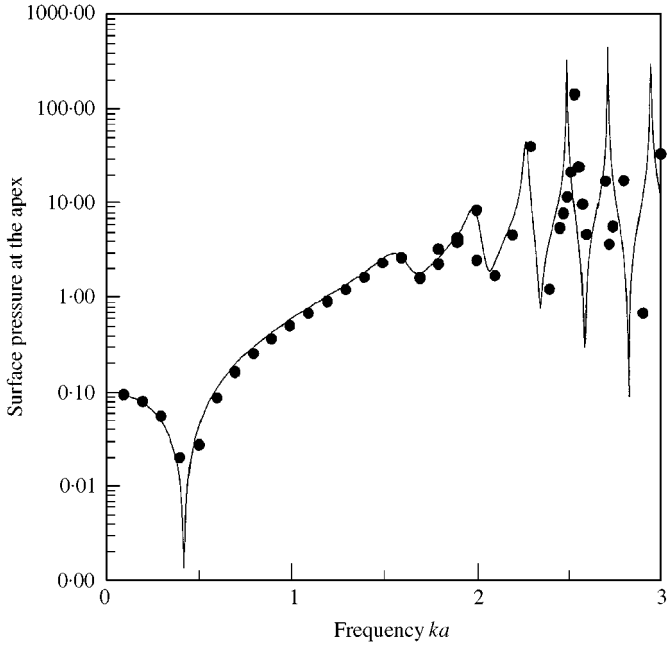

Figure 7. Surface pressure at the apex of the applied point force for the spherical shell versus scanning frequency *ka*. The dotted points are the sampled *ka* values. —— Analytical solution; ● present method.

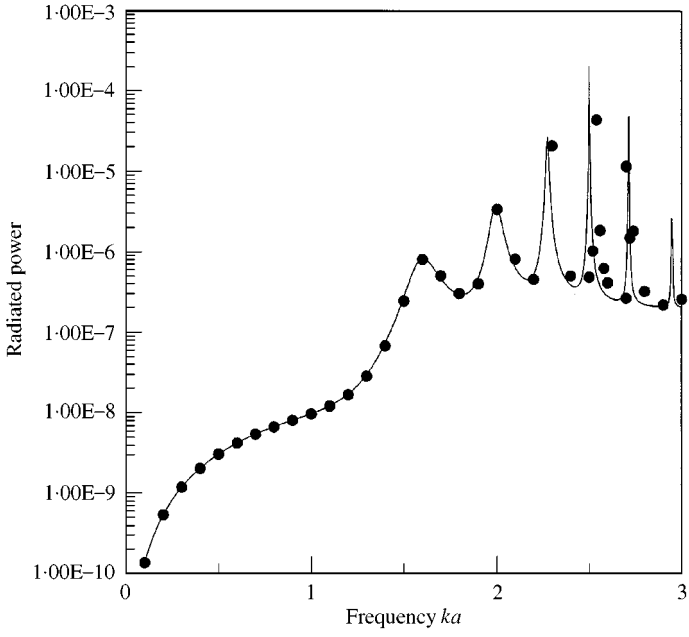

Figure 8. Radiated acoustic power of the spherical shell versus scanning frequency *ka*. The dotted points are the sampled *ka* values. —— Analytical solution; ● present method.

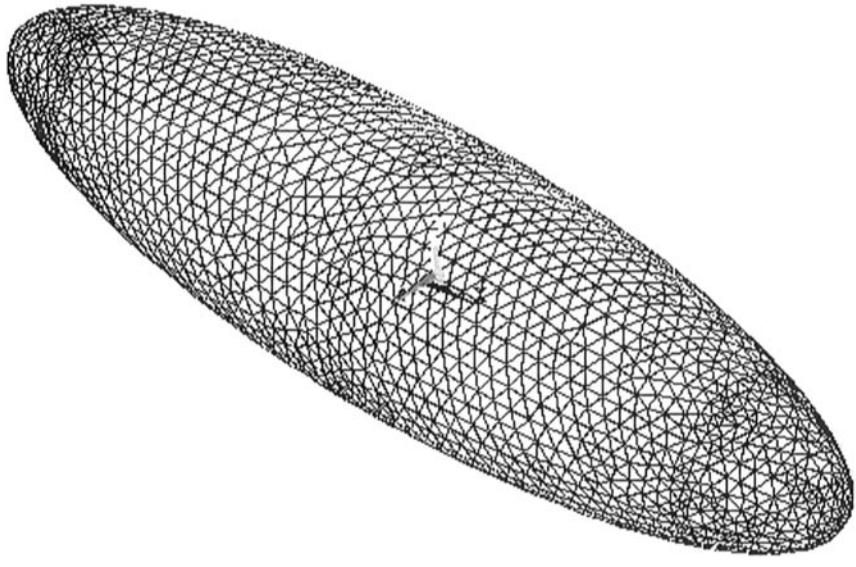

Figure 9. Finite element meshes for a spheroidal shell.

scanned. Figures 13 and 14 show the responses of the surface normal displacement and the surface pressure on the apex of the applied force respectively. Those two plots present errors when *ka* approaches 3 and the error of the surface pressure is larger than the normal displacement. This observation correlates with the general perception that surface pressures

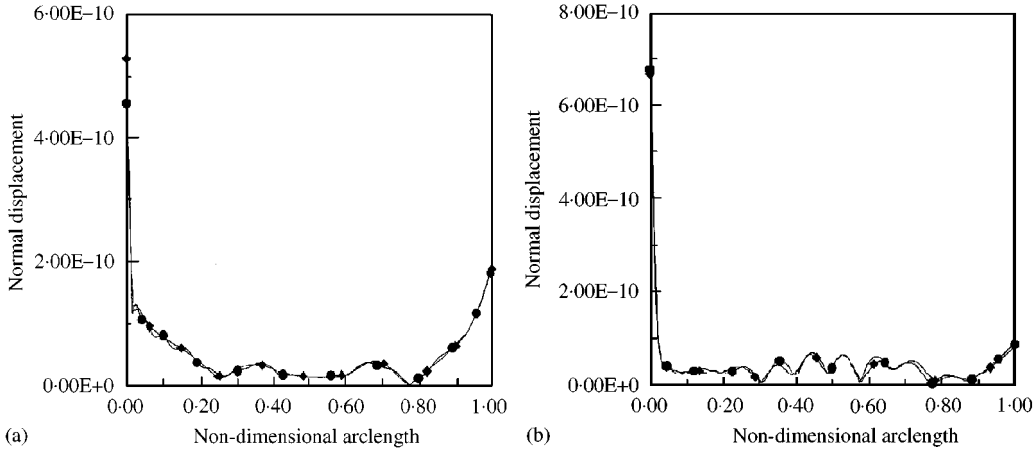

Figure 10. Normal displacement along the arclength of a generator of the spheroidal shell: (a) $ka = 1{\cdot}6$, (b) $ka = 2{\cdot}4$. –●– SVP; –◆– present method.

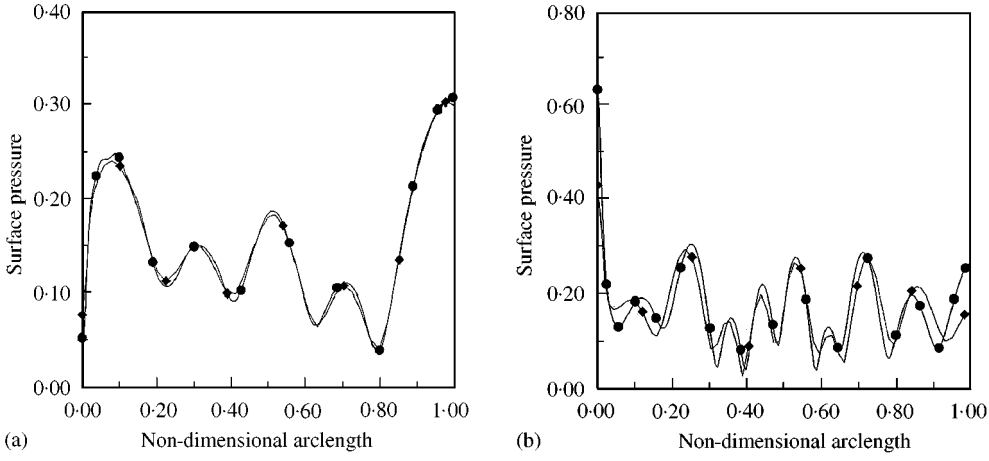

Figure 11. Surface pressure along the arclength of a generator of the spheroidal shell: (a) $ka = 1{\cdot}6$, (b) $ka = 2{\cdot}4$. –●– SVP; –◆– present method.

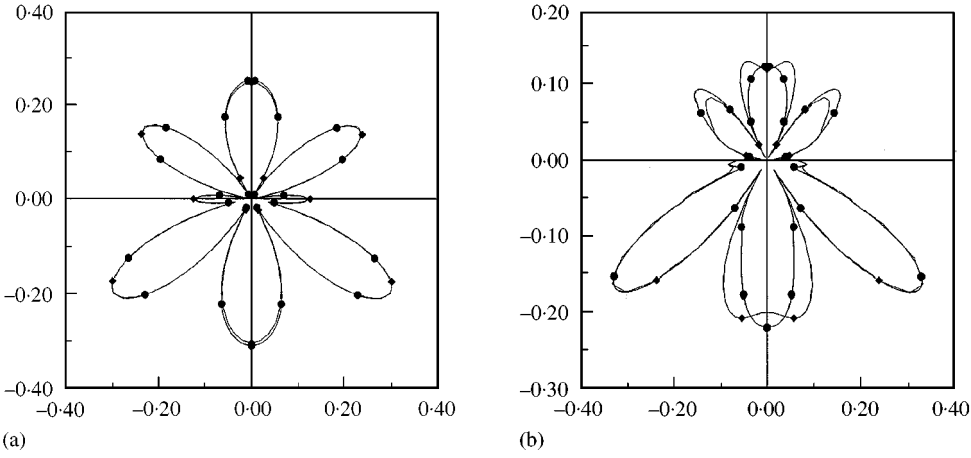

Figure 12. Radiation patterns of the spheroidal shell: (a) $ka = 1{\cdot}6$, (b) $ka = 2{\cdot}4$. –●– SVP; –◆– present method.

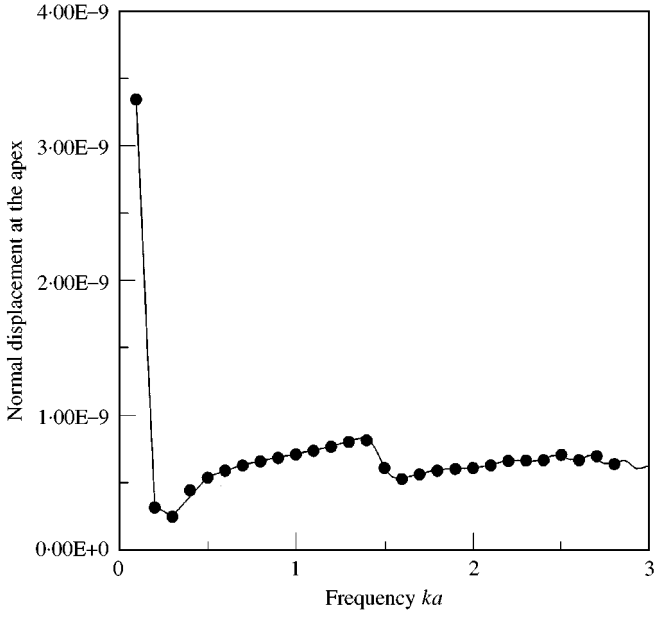

Figure 13. Normal displacement at the apex of the applied point force for the spheroidal shell versus scanning frequency *ka*. The dotted points are the sampled *ka* values. —— SVP; ● present method.

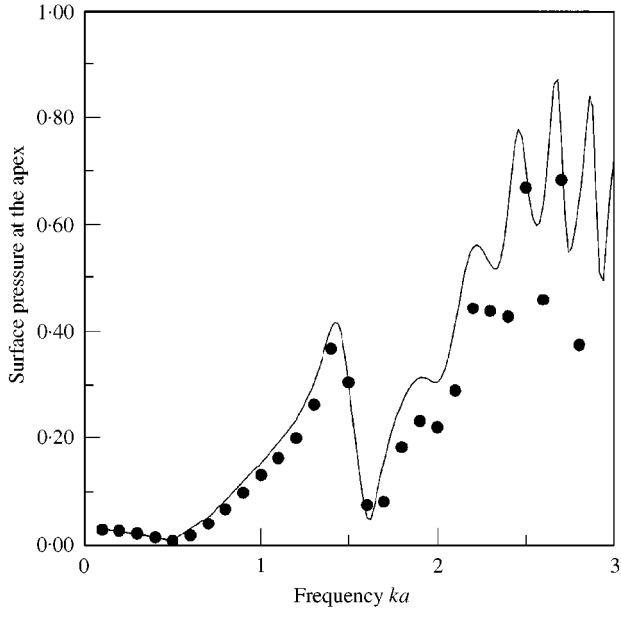

Figure 14. Surface pressure at the apex of the applied point force for the spheroidal shell versus scanning frequency *ka*. The dotted points are the sampled *ka* values. —— SVP; ● present method.

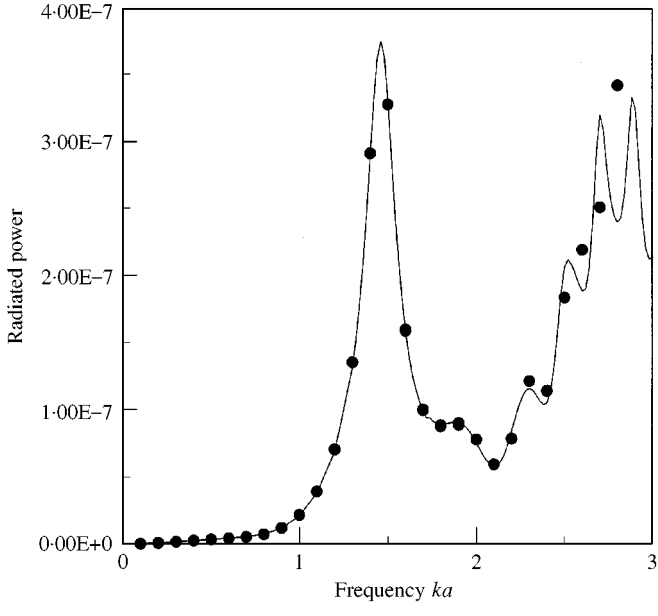

Figure 15. Radiated acoustic power of the spheroidal shell versus scanning frequency *ka*. The dotted points are the sampled *ka* values. —— SVP; ● present method.

usually have more errors than normal displacements. Figure 15 illustrates the radiated power versus the exciting frequency *ka*. Similarly, numerical errors are observed when *ka* approaches 3.

6. COMPUTATIONAL ASPECTS

For problem with a large number of degrees of freedom, the FEM/BEM method frequently requires intensive numerical computations and large memory storage. Therefore, an efficient numerical method should be used. In this study, the computations are performed on a PC with Intel Pentium II CPU and 512 MB memory. The principal computation loads occur at the formation of the acoustic loading element $\rho_0\omega^2 N^{\mathrm{T}}[H]^{-1}[G]$ and solving the system equation of equation (13). The required memory is dominated by storing the matrix elements of equation (13). The efficiency of storing the elements depends on the bandwidth of the system matrix in equation (13). The bandwidth can be reduced by rearranging the ordering of the nodal points based on the Cuthill–Mckee algorithm. Table 1 lists the degrees of freedom of equation (13) and the average bandwidths. It shows that the averaged wavefronts for both numerical examples are small after renumbering as compared with the total degrees of freedom, indicating the effectiveness of matrix storages.

7. CONCLUSIONS

This study presents a novel symmetric formulation for an acoustic loading interacting with submerged elastic structures. The coupled BEM/FEM forms a banded symmetric matrix equation, enabling one to efficiently handle numerical computations and memory allocations. The symmetry of the acoustic loading matrix is demonstrated by a surface

TABLE 1

Bandwidths of the coupled equation (*equation* (13)) *for spherical and spheroidal shells*

	Spherical shell	Spheroidal shell
Total degrees of freedom	19 410	15 804
Average wavefront of the matrix (after renumbering)	467	248
Maximum wavefront of the matrix (after renumbering)	3235	2490

acoustic reciprocal principle in which two sets of surface pressures and normal velocities are related by surface integrals. Also presented herein are two numerical examples subject to point alternating forces which are severe loading conditions in numerical computations rather than surface force conditions. Numerical results are compared with analytical solutions for a spherical shell and variational formulations for spheroidal shells. Comparing numerical data with previously published results demonstrates the efficiency of the proposed method. Moreover, the nature of banded matrix storage provides a highly effective means of handling memory usage as well as computational capacity. Owing to the symmetric formulations and sky-line memory storage, the method proposed herein can handle large-scale problems in a small computer, such as a PC, for more than 10 000 degrees of freedom.

REFERENCES

1. D. T. WILTON 1978 *International Journal of Numerical Methods in Engineering* **13**, 123–138. Acoustic radiation and scattering from elastic structures.
2. I. C. MATHEWS 1986 *Journal of the Acoustical Society of America* **79**, 1317–1325. Numerical techniques for three-dimensional steady-state fluid–structure interaction.
3. R. A. JEANS and I. C. MATHEWS 1990 *Journal of the Acoustical Society of America* **88**, 2459–2466. Solution of fluid–structure interaction problems using a coupled finite element and variational boundary element technique.
4. G. C. EVERSTINE and F. M. HENDERSON 1990 *Journal of the Acoustical Society of America* **87**, 1938–1945. Coupled finite element/boundary element approach for fluid–structure interaction.
5. G. C. EVERSTINE 1991 *Journal of Vibration and Acoustics* **113**, 187–191. Prediction of low frequency vibrational frequencies of submerged structures.
6. P. T. CHEN and J. H. GINSBERG 1995 *Journal of the Acoustical Society of America* **98**, 3343–3351. Complex power, reciprocity, and radiation modes for submerged bodies.
7. H. A. SCHENCK 1968 *Journal of the Acoustical Society of America* **44**, 44–58. Improved integral formulation for acoustic radiation problems.
8. A. J. BURTON and G. F. MILLER 1971 *Proceedings of the Royal Society of London* **323**, 201–220. The application of integral equation methods to the numerical solution of some exterior boundary-value problems.
9. A. GEORGE and J. W.-H. LIU 1981 *Computer Solution of Large Sparse Positive Definite System*, 48–90. Englewood Cliffs, NJ: Prentice-Hall Inc.
10. S. HAYEK 1966 *Journal of the Acoustical Society of America* **40**, 342–348. Vibration of a spherical shell in an acoustic medium.
11. P. T. CHEN and J. H. GINSBERG 1993 *Journal of the Acoustical Society of America* **94**, 221–233. Variational formulation of acoustic radiation from submerged spheroidal shells.